Study on the Impact Wear Characteristics of Catalyst Particles at 90° Elbow via CFD-DEM Coupling Method

X. F. Liu[1], J. F. Zhou[2], S. Q. Gao[1], H. L. Zhao[1], Z. Y. Liao[1], H. Z. Jin[†1] and C. Wang[1]

[1] *Institute of Flow-Induced Corrosion, Zhejiang Sci-Tech University, Hangzhou, Zhejiang, 310018, China*
[2] *Hangzhou Special Equipment Inspection and Research Institute, Hangzhou 310051, China*

†*Corresponding Author Email: haozhe2007@163.com*

ABSTRACT

In the process of petrochemical production, the catalyst particles in the hydraulic conveying pipeline often cause wear failure accidents due to collisions with wall. Compared with spherical particles, non-spherical particles' trajectory would be different due to its geometric shape, and thereby affecting the flow wear characteristics. In this paper, the shape of catalyst particle model with real aspect ratio was constructed by using multi-cluster method, and a CFD-DEM coupling method was adopted by considering the interaction between particle-particle and particle-wall. The study focuses on the effect of particle shape, radius of curvature and angle of bend in terms of the wear characteristics of liquid-solid two-phase flow. The results indicate that with the increase of the particle aspect ratio, the wear rate and the impact density of particles decrease while the impact velocity increases, the wear area of the elbow mainly distributes in the middle part of the outer wall, and its maximum position appears between 78° and 90° in polar coordinates; With the increase of pipe's curvature radius, the main wear area changes due to the direct collision and the sliding friction of the particles along the pipe wall, and its maximum wear rate shows a downward trend due to the reinforce of buffering effect; With the decrease of bending angle, The main wear area decrease because of the changes in particle flow patterns and it is mainly located in the center of the outer wall.

Keywords: Catalyst particles; CFD-DEM; Liquid-solid flow; Non-spherical particles; Numerical simulation.

NOMENCLATURE

Ar	aspect ratio		*Er*	erosion wear rate
D	diameter		*R/D*	radius of curvature
Wr	wear rate		*G*	gravity
α	degree			

1. INTRODUCTION

Solid-liquid two-phase flow is a typical complex multiphase system, which is widely used in chemical, energy, pharmaceutical, metallurgy and other industrial fields (Liu *et al.* 2016). In the residual oil hydrogenation unit of a refining plant, pipelines are used to convey catalyst particles with the liquid oil from catalyst storage tank to the hydrogenation reactor. In the process of transportation, the continuous impact of two-phase fluid on the bend wall causes material loss, wall thinning and bend perforation, which seriously affects the refinery safety. Therefore, to establish the liquid-solid two-phase flow wear prediction method suitable for catalyst particles in the pipe, and obtain the

characteristics of non-spherical particles under different influencing factors as well as the wear distribution is conducive to ensuring the safe and stable operation of the pipeline.

At present, many researches have been done on the particle wear and the feature of flow (Parsi *et al*.2014; Kang and Liu 2020 ; Zolfagharnasab and Salimi 2020; Sedrez *et al.* 2019). Vieira *et al.* (2016) proposed a wall erosion model applicable to different flow rates and particle sizes by combining theory with experiment. Adedeji *et al.* (2019) compared the numerical simulation results with the experimental data of predecessors, and found that

the particle collision angle, velocity and particle mass fraction are the main influencing factors of wear. Singh *et al.* (2019) numerically found that the magnitude and location of maximum erosion wear are more severe in bend rather than the straight pipe. Ou *et al.* (2018) provided a reference for the inspection on the wall thickness of pipeline by numerically study the positions of the maximum wear amount on the elbows. Peng *et al.* (2020) concluded that the most severe erosion area of bend occurred at the elbow exit through analyzing numerical simulation and experimental research. Pei *et al.* (2018) found that changing the curvature radius of elbow directly affects the flow wear characteristics of particles. Zhang *et al.* (2019) took particle collision velocity and angle into account while calculating wear rate.

The aforementioned studies have provided numerically analytical methods, and most of them are based on the assumption of spherical particles in the process of particle model construction. Compared with spherical particles, non-spherical particles' trajectory would be different due to its geometric shape (Christopher *et al.* 2015).

In the study of non-spherical particle flow process, Zhong *et al.* (2009) used spheres to construct non-spherical particles and realized the numerical simulation of the flow behavior of columnar particles in a fluidized bed. Nan *et al.* (2016) and Ma *et al.* (2017) studied the influence of particle length-diameter ratio on convective characteristics through modified columnar particles. Zhou *et al.* (2017) numerically studied the influence of particle shape and turbulence intensity on bend erosion and introduced classic models such as Finne, Oka and E/CR to calculate wear rate. Zeng *et al.* (2018) carried out a simulation of four kinds of shape particles based on DEM framework, introducing shape factor of sphericity to characterize particles, and modifying Oka wear model. Yin *et al.* (2020) analyzed the liquid-solid two-phase flow characteristics of helical blade pipes based on CFD-DEM coupling method. Huang *et al.* (2019) used the CFD-DEM coupling method to study the wear characteristics of the overcurrent part in the centrifugal pump and obtained the wear rate based on the Archard wear model. Li *et al.* (2019) verified the accuracy of CFD-DEM numerical simulation method and the reliability of Archard wear model by comparing simulation and experimental results.

In this paper, a mathematical model for real catalyst particle was established，and a two-way coupling method based on the CFD and DEM methods was adopted to simulate the liquid-solid two-phase flow in catalyst particles conveying pipeline. The Archard wear model is introduced to explore the distribution law of the wear morphology and maximum wear position of the elbow.

2. BOUNDARY CONDITIONS AND COMPUTATION DOMAIN

2.1.1 Process flow and computational domain model

The process of catalyst additions and expulsion system in a company is shown in Fig. 1. Transport oil comes from the fractionation unit and the catalyst comes from the V-8203 fresh catalyst metering hopper. The conveying oil is divided into two channels in the buffer tank, one of which is mixed with the catalyst in V-8203 and pumped into the high-pressure liquid-solid two-phase flow. The other flow is pumped by P-8203 A/B and mixed with a two-phase flow in the transport line. After mixing, it is divided into two channels pumped into R-8101 and R-8102 separately.
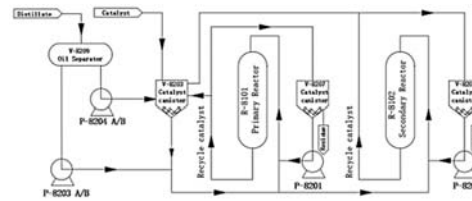

Fig. 1. Process flow diagram of Catalyst addition and drainage system.

In the field of engineering and theoretical research, it is universally accepted that thickness loss on elbows is about fifty times more than that on straight pipelines because of centrifugal force, pressure drop and flow field changes (Nan *et al.* 2015). Therefore, in this paper, particle collision and wear analysis are mainly carried out on the elbow parts of the piping.

The standard geometry model of the computational domain is divided by polyhedral mesh as Fig. 2(b), the inlet diameter D is 80mm in all cases, and the radius of bend is 120mm (1.5D). The upstream and downstream lengths are 10 times the diameter of pipe in order to ensure the full development of liquid-solid two-phase flow. To find the correlation between bend radius of curvature and the flow characteristics, we build 3 other different curvature radiuses of pipeline (R/D = 1, 2, 2.5) as shown in Fig. 2 (a), 2 (c), 2 (d).
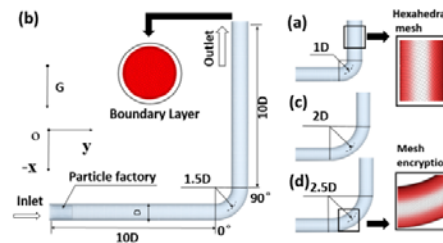

Fig. 2. Pipes with different R/D.

As mentioned above, the shape of the particles affects their flow wear characteristics significantly. Therefore, we model particles with aspect ratio of 5 based on catalyst particles morphology, and in order to study the influence of particle aspect ratio on liquid-solid two-phase flow characteristics, we set 3 other catalyst particles with 4 different aspect ratios as shown in Table 1.

2.1.2 BOUNDARY CONDITIONS

In the CFD calculation, the uniform velocity is applied to boundary condition of the inlet, and the pressure outlet is applied to boundary condition of the outlet. The wall of the entire computational domain is treated as no-slip wall. The near wall mesh is processed using the method of standard wall function. For the discretization calculation of pressure, momentum, turbulent kinetic energy and specific dissipation rate, the second-order upwind scheme is adopted, and the convergence accuracy is set as 1e^{-5}. Columnar catalyst particles are selected for the discrete phase medium, and the particle released velocity is adjusted according to the standard condition. The composition and physical property parameters of the multiphase flow are shown in Table 2.

Table 1 Catalyst particles with different Ar

	Ar=3	Ar=5	Ar=7	Ar=9
Length（mm）	3	5	7	9
Diameter（mm）	1	1	1	1
Aspect ratio（Ar）	3:1	5:1	7:1	9:1
Spheres	5	9	11	13
DEM model				

Table 2 Physical characteristic of oil and particle

Medium	Density (kg/m^{-3})	Viscosity (kg/m^{-1}/s^{-1})	Mass flow rate (kg/s^{-1})	Velocity (m/s^{-1})
Oil	995	6.33e-3	19.3	7.5
Particle	2700	-	1.5	

2.2 CFD-DEM coupling models

In this paper, the CFD-DEM coupling method is used to simulate the collision process between particle-particle and particle-wall in the liquid-solid two-phase flow (Januário and Maia 2020). For the calculation of the continuous phase flow field, the RNG k-ε turbulent model is adopted. The soft ball model is used to simulate the collision motion behavior of particles in the liquid, and the erosion is calculated by the Archard model (Ren *et al.* 2012).

2.2.1 Continuous phase model

(1) Continuity equation:

$$\frac{\partial}{\partial t}(\alpha_f \rho_f) + \frac{\partial}{\partial x_j}(\alpha_f \rho_f u_j) = 0 \quad (1)$$

(2) Momentum equation:

$$\frac{\partial}{\partial t}(\alpha_f \rho_f u_i) + \frac{\partial}{\partial x_j}(\alpha_f \rho_f u_i u_j) =$$

$$-\frac{\partial p}{\partial x_i} + \frac{\partial}{\partial x_j}\left[\alpha_f \mu_{eff}\left(\frac{\partial u_i}{\partial x_j} + \frac{\partial u_j}{\partial x_i}\right)\right] + \alpha_f \rho_f g + F_S \quad (2)$$

Where ρ_f is the fluid density, u is the velocity, p is the pressure, μ_{eff} is the mixed viscosity, g is acceleration of gravity, F_s is the interaction term due to the force between the particles and the fluid.

Turbulence model selected RNG $k - \varepsilon$, it is based on the standard $k - \varepsilon$ model:

$$\frac{\partial}{\partial t}(\rho k) + \frac{\partial}{\partial x_j}(\rho k u_i) =$$

$$\frac{\partial}{\partial x_j}(\alpha_k \mu_{eff}\frac{\partial k}{\partial x_j}) + G_k + G_b - \rho\varepsilon - Y_M + S_k \quad (3)$$

$$\frac{\partial}{\partial t}(\rho\varepsilon) + \frac{\partial}{\partial x_i}(\rho\varepsilon u_i) = \tag{4}$$

$$\frac{\partial}{\partial x_j}(\alpha_k\mu_{eff}\frac{\partial k}{\partial x_j}) + C_{1\varepsilon}\frac{\varepsilon}{k}(G_k + G_{3\varepsilon}G_b) - C_{2\varepsilon}\rho\frac{\varepsilon^2}{k} - R_\varepsilon + S_\varepsilon$$

Where G_k and G_ω represents the production of turbulent kinetic energy k, Y_M represents the loss of M caused by turbulence, S_k and S_ε represents the source term.

2.2.2 Discrete phase model

In this paper, the particle motion law is described by Newton's second law of motion, the relevant kinetic calculation equation is as follows:

$$m\frac{dv}{dt} = mg + \sum F_C + F_{drag} + F_b + F_m + F_{sl} \tag{5}$$

$$I\frac{d\omega}{dt} = \sum T_c + T_f \tag{6}$$

Where F_C and F_{drag} represents contact force, fluid drag force, Basset force, Magnus force, Saffman lift force. m and I are the mass and moment of inertia of the particle. $d\omega/dt$ is the translational acceleration of the particle. T_c and T_f are the torque produced by the contact and fluid phases, respectively.

In this paper, the soft ball model as shown in Fig. 3 is adopted to reveal the interaction generated by particle collision. Particle I and particle J have contact collision at point C, forming deformation of δ_n and δ_t in the normal and tangential magnitude. After collision, the particles produce normal and tangential forces $Fc.n$、$Fc.t$.
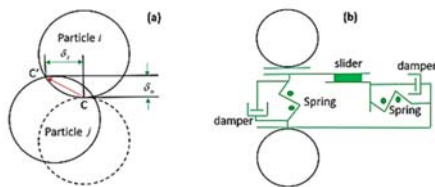
Fig.3. (a) Normal displacement δ_n and tangential displacement δ_t of particle collision; (b) constitutive model of the interaction between two particles.

$$F_{con} = -k_n\delta_n - \eta_n v - k_t\delta_t - \eta_t v_t \tag{7}$$

Spring and damping in Fig. 3 (b) can simulate deformation damping and damping effect, respectively. Sliding plate can simulate the sliding friction effect.

The motion resistance coefficient of no-spherical particles Cd_0 in continuous phase fluid is related to

Reynolds number:

$$Cd_0 = \frac{24}{Re_p}(1 + b_1 Re_p^{b2}) + \frac{b_3 Re_p}{b_4 + Re_p} \tag{8}$$

The Archard Wear (Archard *et al.* 2004) was developed based on Hertz-Mindlin (No slip) model. Its expression is:

$$Q = W P d_t \tag{9}$$

Where Q is the wear volume (mm³), and d_t is the tangential movement distance (mm) of particles, and P is the applied load (N). The wear constant W is expressed as follows:

$$W = \frac{K}{H} \tag{10}$$

Where, H is the surface hardness of the contact material, and K=10^{-11} according to the experimental data of Chen (Chen *et al.* 2017). Wall wear thickness h can be calculated by:

$$h = \frac{Q}{A} \tag{11}$$

Where, A is the contact area between solid particles and wall surface.

2.3. Model validation

The computation domain and control equations are discredited using finite volume method. To ensure that the calculation result is not affected by the mesh number and to save computing resources, three sets of meshes were selected to verify the mesh independent. As shown in Table 3, with the increases in the number of mesh, the change of maximum elbow erosion is less than 1.5%, which is thought to have achieved the mesh independence requirement. Therefore, the number of computation domain mesh is finally determined as 1.2 million.

Table. 3. Mesh independence verification

| Mesh number (10^5)	Max wear rate (mm·s⁻¹)	Relative variation (%)
8	4.99e-5	--
12	5.05e-5	1.20
16	5.10e-5	0.99

In the verification process of the numerical prediction method, we selected Li Yi's research results (Li *et al.* 2019) for comparative analysis, taking the maximum wear rate and average wear rate under different particle mass concentrations as the characterizing parameters. The particle concentration

range is 1% to 15%, and the corresponding discrete phase particle mass flow rate at each mass concentration is different by setting the particle mass flow rate in EDEM, Fig. 4 is a comparison between the calculation results of the numerical prediction model constructed in this study and Li Yi's experimental results and simulation results. The observation chart shows that the numerical calculation results are consistent with the changes in Li Yi's research results, as the particle mass concentration changes from 1% to 9%, the wear rate of the test piece gradually increases, but when the particle mass concentration is greater than 9%, the
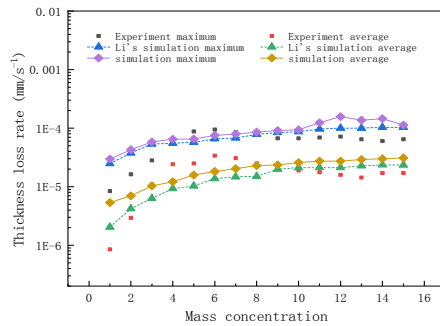
Fig. 4. Wear rate for different particle concentrations.

changes in wear rate are slighter than before. This phenomenon can be explained by the buffer effect proposed by Duarte *et al.* (2016): When the concentration of particles increases to a certain level, a layer of flowing particle barriers will be formed on the pipe wall, effectively prevent wear loss caused by direct collision between particles and wall surface.
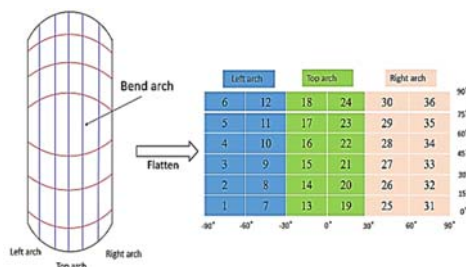
**Fig. 5. Statistical domain of the elbow's outer wall.**

3. RESULTS AND DISCUSSION

A large number of studies have found that erosion of liquid-solid two-phase flow at elbow mainly occurs at the middle and sides of outer wall (Li *et al.* 2019, Singh *et al.* 2019, and Anna *et al.* 2020). Therefore,

for the convenience of statistical data, the outer wall of the elbow is divided into 33 zones along the polar coordinates from 0 to 90 degrees. As shown in Fig. 5: 1-11, 12-22, 23-33 are arranged on the left, middle and right sides of the outer wall in turn, respectively.

3.1 Effects of particle's Ar

Figure 6 (a) shows particles in the flow are mainly affected by drag force, gravity and contact force of fluid (Ma *et al.* 2017). When the aspect ratio grows, the impact frequency for a particle decreases in elbow. This is because particles with lager Ar will increase the distance between the two adjacent vertices and lead to a longer path to complete a collision for them. Figure 6 (b) shows the distribution of particles with different aspect ratio in the elbow, the particles with aspect ratio of 3 are most evenly distributed in the elbow, and with the increase of the aspect ratio, the probability of collision between particles increases which results in a more dispersed particle distribution. After the first collision, most particles will roll and rebound along the outer wall of the elbow. In the process of rebound, they will collide with the later particles and hit the elbow again along the outer wall. Due to the increase of the windward area of particles with large Ar, the drag force of the fluid received by the particles is stronger. At the same time, because the particle's trajectory increases, its acceleration time is longer. Therefore, compared with particles with a small Ar, particles with lager Ar have a greater wall impact velocity. The detailed analysis of the relationship between velocity and particle frontal area is provided in jia-wei Zhou literature (Zhou *et al.* 2017). Figure7 is the statistical date of four different Ar particles in each elbow (the same mass flow rate and constant density). The number of particles with large aspect ratio decreases due to the increase of its weight. In conclusion, the impact density of particles decreases with the increase of aspect ratio, while the impact velocity increases with the increase of aspect ratio.
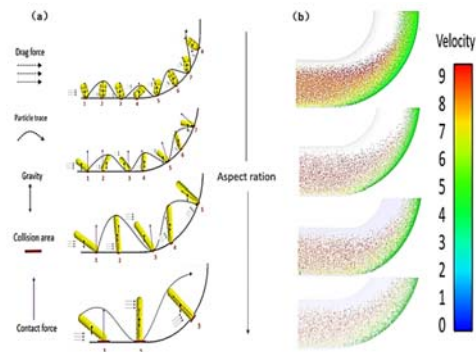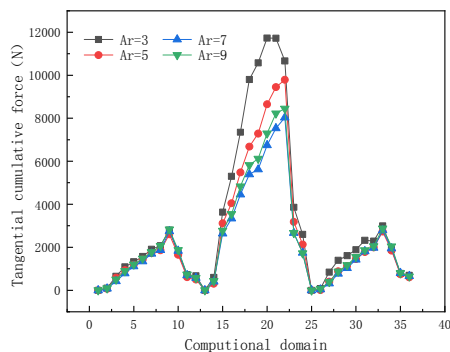

Fig. 6. Motion process of particles with different Ar in an elbow: (a) the schematic of particle motion in an elbow, (b) Particle velocity contours.
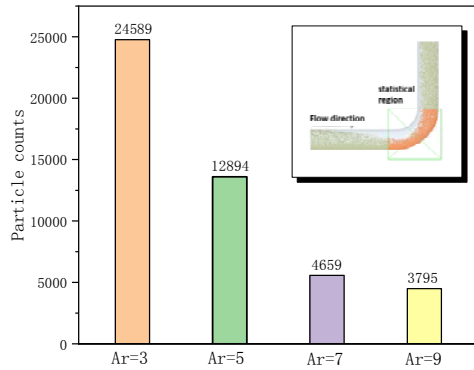
Fig. 7. Statistical date of four different Ar particles in each elbow.
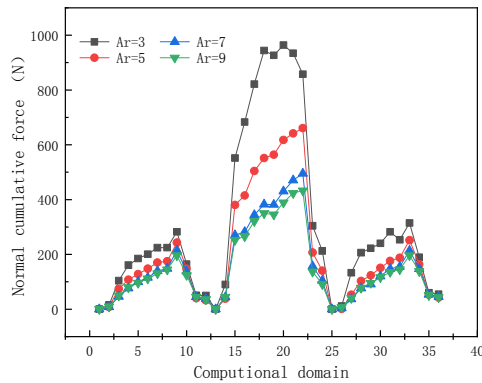

Fig. 8(a) Normal cumulative force.

Fig. 8(b) Tangential cumulative force.

Figure 8 shows the cumulative force of 4 different aspect ratio particles on the elbow wall. The cumulative impact force of the particles on the wall decreases with the increase of the aspect ratio, but the impact force formed by the four particles has similar wave forms in the calculation domain. The three segments of parabola all start from plane 0°, increase continuously along the polar coordinate direction,

and then fall down after reaching the maximum value near the plane 80°. The maximum values of the normal accumulative force and tangential accumulative force appear in the middle part of the outer wall, and reach 987N and 12000N, respectively. In summary, the impact cumulative force of particles with large aspect ratio on the wall surface is less than that of particles with small aspect ratio. The maximum accumulated collision force is located near the polar coordinate plane of 80°, and the tangential accumulated force on the pipeline wall is far greater than the normal one.

Figure 9 is the statistical chart of the erosion for different particles on the elbow. The wear rate of elbow decreases with the increase of length-diameter ratio of particles. The wear curves formed by the four particles are similar, and the maximum wear position appears near the polar coordinate plane of 80°. The particles with an aspect ratio of 3 have the maximum wear amount of 1.0×10^{-5}mm/s at position 22.
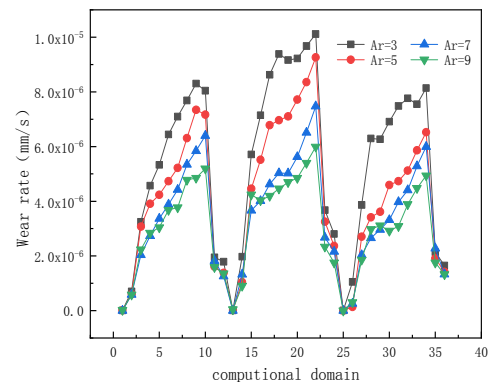

Fig. 9. Influence of particle Ar on elbow wear rate.

3.2 Effects of curvature radius

In this part, elbows with four different radii of curvature (R/D=1, 1.5, 2and 2.5) are chosen based on actual working condition. The particle aspect ratio is set as Ar=5, and pipe diameter is set as D=80mm.

Figure10 shows that the flow characteristics of particles in the pipe. It can be divided into three stages: the accelerated motion in the inlet straight pipe section, the collision decelerated motion in the elbow section and the decelerated motion in the outlet straight pipe section. It can be seen that under the action of centrifugal force in the elbow, low-speed particle flow is formed along the outer wall of the pipe after collision. The particle group gradually disperse after flowing out of the elbow, and its dispersion velocity decreases with the increase of R/D. The particle flow distance along the outer wall increases with the increase of the curvature radius, and the position of collision in the inner side of the vertical tube also rose which results in the increase of the collision area at the outer wall.
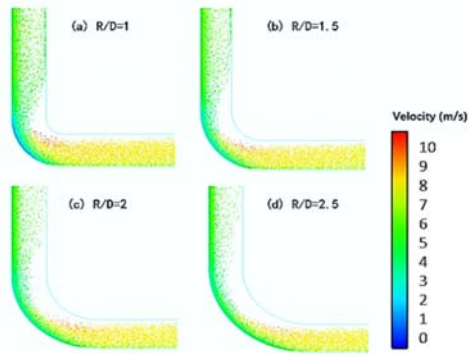
**Fig. 10. Particle motion in four different curvature radius elbows.**

A Poincare Map was used to visualize the particle trajectories in the different curvature radius elbows as shown in Fig. 11. By Analyzing Fig. 11(b), (c), and (d), with the increase of the radius of curvature, the number of particles flowing through the middle of the pipe decreases continuously, while the thickness of particles flowing on the outside wall decreases obviously. This is because the fluid motion changes more violently in the pipe with a small radius of curvature, and the particle motion does not have enough time to adapt to the change and directly flow out of the elbow after the collision with the pipe wall.\
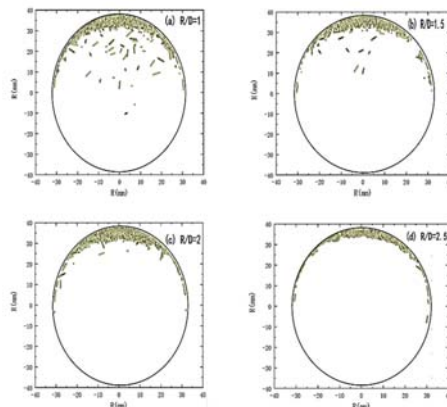
**Fig. 11. Poincare Map of particles with different curvature radius in the elbow.**

Figure12 shows the erosion distributions in different elbow. As the R/D increases, the main wear part is shifted towards the entrance of the elbow and the whole erosion area gradually increases due to simultaneous work of direct impact and sliding friction of particles along the pipe wall. With the increase of the bending length of the pipe, the number of sliding friction and collision between the particles and the pipe wall will increase, and the distribution of the particles will be more dispersed, which leads to a larger erosion and thinning range of the pipe wall and the erosion area become dispersed. And, the

particles slide on the wall and tend to appear at higher wear rates, resulting in more erosion peaks, as shown in Fig. 12.
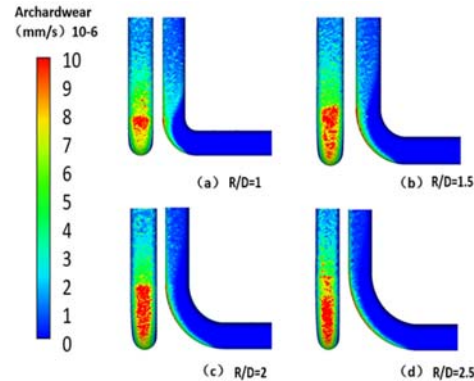
Fig. 12. Erosion distributions in different elbows.

Statistics of the maximum wear rate of the outer wall of the four different curvature radii are shown in Fig. 13. The maximum wear amount decreases with the increase of the curvature radius of the elbow. This is because particles cost more time flowing through the elbow with large R/D bend and the flow structure formed by them are more compact which results in direct collision times decreases between the particles and wall.
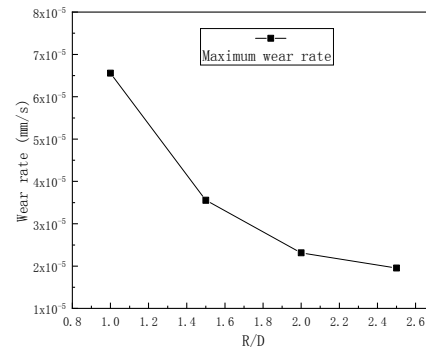

Fig. 13. Maximum wear rate of four elbows with different R/D.

3.3 Effects of bending angle

In this part, elbows with five different bending angle ($\alpha_1/\alpha_2/\alpha_3/\alpha_4/\alpha_5$ =150°/120°/90°/60°/30°) are constructed to numerically study the influence of bending Angle on the wear characteristics of liquid-solid two-phase flow as shown in Fig. 14.

Figure 15 shows the particle movement inside the elbow with 5 different bending angles. Through the analysis of the cloud diagram, it can be known that as the bending angle decreases from 150° to 90°, The influence of channel shape on particle velocity is reduced, and more particles will flow with the liquid phase, reducing the friction between the particles and
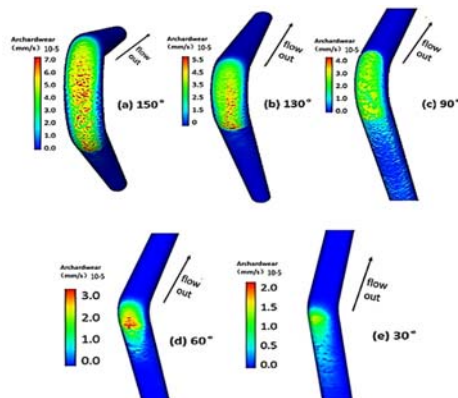
the outer wall of the pipe; as the bending angle further decreases from 90°, the channel shape tends to be straight, the impact angle of the particles on the outer wall of the pipe will decrease. And the liquid flow rate will continue to increase, so that the particles are evenly distributed inside the pipe and the trajectory is gradually parallel to the axis. As the velocity of the fluid continues to increase, the particles are evenly distributed inside the pipe and the trajectories are gradually parallel to the axis.
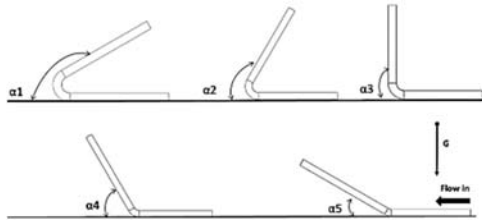
Fig. 14. Diagram of elbows with different bending angles.
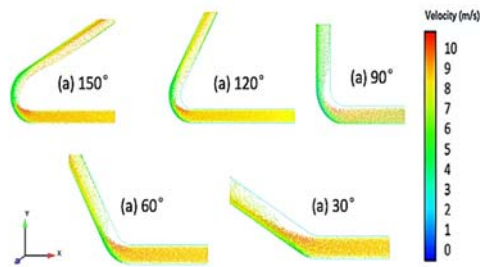
Fig. 15. Particle motion in five different bending elbows.

Fig. 16. Contours of wear rate on the outer wall.

Figure 16 shows the Contours of wear on the outer

wall with different bending angles, with the decrease of the bending angle, the wear area of the outer wall of the elbow gradually decreases. The maximum erosion wear area of each elbow is located in the center of the outer wall. This is because under the action of the centrifugal force of the elbow, the velocity of particles there is greater than that of particles near the wall, resulting in the increase of the final collision loss.

Figure 17 is the statistical data of the maximum wear on the outer wall of each elbow, a decrease in the bending angle can dramatically reduce the maximum wear rate.

4. CONCLUSION

In this paper, the flow characteristics of catalyst particles in the 90° bend of catalyst addition in hydrogenation reactor were numerically simulated. The method of CFD-DEM coupling was used to simulate the column catalyst particles in the pipeline. Archard wear model was also used to study the erosion of the elbow. The main conclusions are as follows:

(1) The impact density of particles decreases with the increase of Ar, while the impact velocity increases with the increase of Ar. The main wear area of the elbow has little effect by the change of Ar, but the wear rate is positively correlated with the impact force. The maximum erosion position occurs between 78° and 90° in polar coordinates.
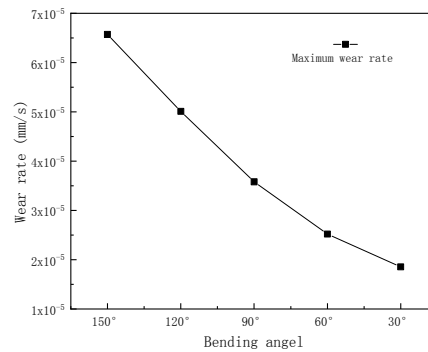
Fig. 17. Maximum wear rate of five elbows with different bending angle.

(2) The increase of elbow curvature radius leads to the increase of the particle collision distance along the outer wall which results in an increase of the collision area. The major cause of erosion is simultaneously work of direct impact and sliding friction of particles along the pipe wall, and its the maximum wear rate shows a downward trend due to the reinforce of buffering effect.

(3) The main wear area of the elbow's outer wall and its maximum wear amount decreases as the reduction

of bending angle. The maximum wear area of each elbow is located in the center of the outer wall, this is because under the action of the centrifugal force of the elbow, the velocity of particles there is greater than that of particles near the wall, resulting in the increase of the final collision loss.

REFERENCES

Adedeji, O. E., W. Yu and R. S. Sanders (2019). Analysis of local wear variables for high-precision erosion modeling in complex geometries. *Wear* 426, 562-569.

Anna, K., B. V. Balakin and P. Kosinski (2020).Theoretical analysis of erosion in elbows due to flows with nano- and micro-size particless. *Powder Technology* 333, 47-59.

Archard, J. F. (2004). Contact and Rubbing of Flat Surfaces. *Journal of Applied Physics* 24(8), 981-988.

Chen, G., Y. Liu and G. Lodewijks (2017). Experimental research on the determination of the coefficient of sliding wear under iron ore handling conditions. *Tribology in Industry* 39(3), 378-390.

Christopher B. Solnordal and Y. Chong (2015). An experimental and numerical analysis of erosion caused by sand pneumatically conveyed through a standard pipe elbow. *Wear* 336, 43-57.

Duarte, C., F. Souza and R. Salvo (2016). The role of inter-particle collisions on elbow erosion. *International Journal of Multiphase Flow* 89, 1-22.

Huang, S., J. Huang and J. Guo (2019). Study on Wear Properties of the Flow Parts in a Centrifugal Pump Based on EDEM–Fluent Coupling. *Processes* 7(7), 431.

Januário, J. R. and C. B. Maia (2020). CFD-DEM Simulation to Predict the Critical Velocity of Slurry Flows. *Journal of Applied Fluid Mechanics* 13(1), 161-168.

Kang, R. and H. Liu (2020). An integrated model of predicting sand erosion in elbows for multiphase flows. *Powder Technology 366.*

Li, Y., H. Zhang and Z. Lin (2019). Relationship between wear formation and large-particle motion in a pipe bend. *Royal Society Open Science* 6(1) 181254.

Liu, X., W. Zhong and A. Yu (2016). Mixing behaviors in an industrial-scale spout-fluid mixer by 3D CFD-TFM. *Powder Technology* 314,455-465.

Ma, H., L. Xu and Y. Zhao (2017). CFD-DEM simulation of fluidization of rod-like particles in a fluidized bed. *Powder Technol* 314, 355-366.

Nan, L. and H. Lan (2015). Effect of the gas–solid two-phase flow velocity on elbow erosion. *Journal of Natural Gas Science and Engineering* 26, 581-586.

Nan, W., Y. Wang and J. Wang (2016). Numerical analysis on the fluidization dynamics of rod like particles. *Adv Powder Technol* 27(5), 2265-2276.

Ou, G., K. Bie and Z. Zheng (2018). Numerical simulation on the erosion wear of a multiphase flow pipeline. *International Journal of Advanced Manufacturing Technology* 96(5-8), 1705-1713.

Parsi, M., K. Najmi and F. Najafifard (2014). A comprehensive review of solid particle erosi on modeling for oil and gas wells and pipelines applications. *Journal of Natural Gas Science and Engineering* 21, 850-873.

Pei, J., A. Lui and Q. Zhang (2018). Numerical investigation of the maximum erosion zone in elbows for liquid-particle flow. *Powder Technology* 333, 47-59.

Ren, B., W. Zhong, and Y. Chen (2012). CFD-DEM simulation of spouting of corn-shaped particles. *Particuology* 10(5), 562-572.

Sedrez, T. A., S. A. Shirazi and Y. R. Rajkumar (2019). Experiments and CFD simulations of erosion of a 90° elbow in liquid-dominated liquid-solid and dispersed-bubble-solid flows. *Wear* 426, 570-580.

Singh, V., S. Kumar and S. K. Mohapatra (2019). Modeling of Erosion Wear of Sand Water Slurry Flow through Pipe Bend using CFD. *Journal of Applied Fluid Mechanics* 12(3), 679-687.

Vieira, R. E., A. Mansouri and B. S. Mclaury (2016). Experimental and computational study of erosion in elbows due to sand particles in air flow. *Powder Technology* 288, 339-353.

Yin, J., Q. Y. Chen, R. Zhu and W. X. Tang (2020). Enhancement of Liquid-Solid Two-Phase Flow Through a Vertical Swirling Pipe. *Journal of Applied Fluid Mechanics* 13(5), 1501-1513.

Zeng, D. Z. and E. B. Zhang (2018). Investigation of erosion behaviors of sulfur-particle-laden gas flow in an elbow via a CFD-DEM coupling method. *Powder Technology* 329, 115-128.

Zhang, R.，H. Li and S. Dong (2019). Approximate

theoretical solution of the movement and erosion of solid particles in a 90°bend. *Wear* 430-432.

Zhong, W. Q., Y. Zhang and B. S. Jin (2009). Discrete Element Method simulation of cylinder-shaped particle flow in a gas- solid fuidized bed. Chemical Engineering & Technology 32(3), 386-391.

Zhou, J. W., Y. Liu and S. Y. Liu (2017). Effects of particle shape and swirling intensity on elbow erosion in dilute-phase pneumatic conveying. *Wear* 380-381, 66-77.

Zolfagharnasab, M. H. and M. Salimi (2020). A novel numerical investigation of erosion wear over various 90-degree elbow duct sections. *Powder Technology* 380, 1-3.